Title

An allograft mouse model for the study of hearing loss secondary to vestibular schwannoma growth

Journal

JOURNAL OF NEURO-ONCOLOGY, 129(1)

ISSN

0167-594X

Authors

Bonne, N-X
Vitte, J
Chareyre, F
et al.

Publication Date

2016-08-01

DOI

10.1007/s11060-016-2150-9

Peer reviewed

An allograft mouse model for the study of hearing loss secondary to vestibular schwannoma growth

Nicolas-Xavier Bonne, Jérémie Vitte, Fabrice Chareyre, Gevorg Karapetyan, Vazgen Khankaldyyan, Karo Tanaka, Rex A. Moats, et al.

Journal of Neuro-Oncology

ISSN 0167-594X

J Neurooncol
DOI 10.1007/s11060-016-2150-9

Springer

J Neurooncol
DOI 10.1007/s11060-016-2150-9

LABORATORY INVESTIGATION

An allograft mouse model for the study of hearing loss secondary to vestibular schwannoma growth

Nicolas-Xavier Bonne[1,2] · Jérémie Vitte[3,4] · Fabrice Chareyre[1] · Gevorg Karapetyan[5] · Vazgen Khankaldyyan[5] · Karo Tanaka[1] · Rex A. Moats[5] · Marco Giovannini[3,4]

Received: 19 October 2015 / Accepted: 6 May 2016

Abstract Vestibular schwannoma is a benign neoplasm arising from the Schwann cell sheath of the auditory-vestibular nerve. It most commonly affects both sides in the genetic condition Neurofibromatosis type 2, causing progressive high frequency sensorineural hearing loss. Here, we describe a microsurgical technique and stereotactic coordinates for schwannoma cell grafting in the vestibular nerve region that recapitulates local tumor growth in the cerebellopontine angle and inner auditory canal with resulting hearing loss. Tumor growth was monitored by bioluminescence and MRI in vivo imaging, and hearing assessed by auditory brainstem responses. These techniques, by potentially enabling orthotopic grafting of a variety of cell lines will allow studies on the pathogenesis of tumor-related hearing loss and preclinical drug evaluation, including hearing endpoints, for NF2-related and sporadic schwannomas.

✉ Marco Giovannini
mgiovannini@mednet.ucla.edu

[1] House Research Institute, Center for Neural Tumor Research, Los Angeles, CA, USA

[2] Department of Otology and Neurotology, University Hospital of Lille, and INSERM U1008 "Controlled Drug Delivery System and Biomaterials", University of Lille, Lille, France

[3] Department of Head and Neck Surgery, University of California Los Angeles, David Geffen School of Medicine at UCLA, Los Angeles, CA, USA

[4] Jonsson Comprehensive Cancer Center, University of California Los Angeles, David Geffen School of Medicine at UCLA, Los Angeles, CA, USA

[5] Department of Radiology, USC Keck School of Medicine, The Saban Research Institute of Children's Hospital Los Angeles, Los Angeles, CA, USA

Keywords Neurofibromatosis type 2 · Vestibular schwannoma · Auditory brainstem response · Mouse model

Introduction

Vestibular schwannomas (VS) are intracranial, extra-axial tumors that arise from the Schwann cell sheath of the 8th cranial nerve. As VS increase in size, they eventually occupy a large portion of the cerebellopontine angle. Over 3300 vestibular schwannomas are diagnosed per year in the US and incidence is 1.09 per 100,000 population [1]. The great majority of VS are sporadic unilateral, which usually develop between ages 40 and 60. About 5 % of VS are bilateral and occur in neurofibromatosis type 2 (NF2), an autosomal dominant genetic disease [2]. The NF2 tumor suppressor gene [3, 4], is inactivated in both NF2-associated and sporadic VS [5, 6]. At presentation, more than 90 % of NF2 patients demonstrate some change in hearing on the side of a VS [7], with the usual audiogram describing a high-frequency slope in more than 60 % [7, 8].

The mechanisms underlying deafness in NF2 are still unclear and are supposed to be multifactorial [9, 10]. Tumor size and increase in tumor volume are not correlated to hearing status [7, 9, 11], but multiple changes affecting the cochlea correlate with hearing level in these patients [12, 13]. It was also suggested that differences in the course of hearing might result from genetic determinants intrinsic to the tumor [14].

Increased interest in developing new strategies for the treatment of VS, in particular for those occurring in the context of NF2, results in an increasing requirement for accurate mouse models recapitulating the tumor natural history of the human condition [15]. Moreover, the use of

Published online: 13 May 2016

anti-angiogenic drug therapy has suggested a beneficial effect on hearing, an endpoint that is overlooked in the preclinical field [16]. Thus, a better understanding of the process underlying hearing loss requires specific models. Although accurately reproducing some of the manifestations of NF2, genetically engineered mouse models (GEM) are time and resources consuming, therefore best suited in validating promising therapies rather than for high throughput drug screening [15]. As an alternative, orthotopic grafting techniques can be used to recapitulate biologically relevant tumor growth and microenvironment [17]. Here, we describe a new in vivo modeling approach for VS based on orthotopic grafting of NF2-deficient Schwann cells in the auditory-vestibular nerve complex region. By growing in the cerebellopontine angle and inner auditory canal, these tumors reproduce some of the features of human VS, including progressive hearing loss, providing a new functional endpoint for high throughput preclinical NF2 drug screening.

Material and methods

Cell line

The SC4 Schwann cell line was derived from adeno-Cre-infected, spontaneously transformed Schwann cells isolated from adult $Nf2^{KO3/flox2}$ mouse sciatic nerve in the FVB/N background [18–21]. SC4 cells were transfected with a plasmid encoding a fusion EGFP-luciferase gene under the control of the CMV promoter, and stable cell clones were selected using cell sorting. The clone SC4-9*luc* used for these studies was serially passaged in vitro.

Mice

Athymic immunodeficient NU-$Foxn1^{nu}$ (NU/NU) mice in an outbred BALB/C background were obtained from Charles River Laboratories. All animal care and experimentation reported here were conducted in compliance with the guidelines and with the specific approval of Institutional Animal Care and Use Committee under protocol numbers HEI1175-08-03 and CHLA315-12.

Microsurgery approach to the cerebellopontine angle to access the auditory-vestibular nerve complex

Following anesthesia by intraperitoneal administration of xylazine (10 mg/kg) and ketamine-HCl (100 mg/kg), the left post-auricular region was shaved and cleaned for surgical approach. Under the operating microscope, after a semi-circular incision was made extending from the vertex to the neck, an auricular flap was elevated anteriorly to give access to the lateral skull base including the petrous bone and occipital bone. Nuchal muscles were elevated and the sterno-cleido-mastoidian insertions separated from the lateral aspect of the petrous bone. The facial nerve was then identified as it exited the skull base. To avoid bleeding, the exposed bone was cauterized. Identification of the lateral and posterior semicircular canals and root of the zygoma anteriorly defined the drilling area (Fig. 1a–c). A 0.6 mm diamond was used to drill the bone overlying the dura mater covering the flocculus of the cerebellum. A maximal exposure was obtained by lining both semi-circular canal and the lateral sinus, the dura was opened and the flocculus retracted posterior-superiorly allowing access to the cerebellopontine angle. The arachnoidal layer of the cysterna pontis would eventually open spontaneously or it was punctured using a sharp hook, the cerebrospinal fluid was then allowed to drain. Transparency of the ampullae, situated close to the nerve, allowed targeting the auditory-vestibular nerve complex at the porus for injection. The craniotomy was then occluded using bone wax for a waterproof closure. The total surgery duration was approximately 25 min.

Stereotactic approach to the auditory-vestibular nerve complex

Stereotaxic coordinates in 8-week-old NU/NU mice were established in a preliminary trial by injecting India ink through the cannulas followed by a postmortem histological examination.

The stereotactic device (Stoelting Lab standard rat stereotaxic instrument (#51600) with mouse adapter (#51624)) was calibrated to precisely target the inner auditory canal in the area of the vestibular ganglion, next to the auditory-vestibular nerve complex, and identified and validated specific coordinates: 4.91 mm cranio-caudal from the bregma, 2.1 mm lateral from the midline and 5.6 mm in depth from the surface of the skull.

Injection procedure

The injection method developed in this protocol was modified from Wu et al. 2005 [22]. SC4-9*luc* cells were suspended in Dulbecco's Modified Eagle Medium (D-MEM, Life Technologies) containing 10 % FBS at a concentration of 4.16×10^5/µl allowing injection of 5×10^4 cells in 120 nl. Following microsurgery or stereotactic approach, the cell suspension (or the cell-free medium for sham injections) was infused gradually in the left auditory-vestibular nerve complex at a rate of 1 nl/s (UMPIII micropump, Micro 4 microprocessor, World Precision Instruments) using the Intra Ocular Injection Kit (World

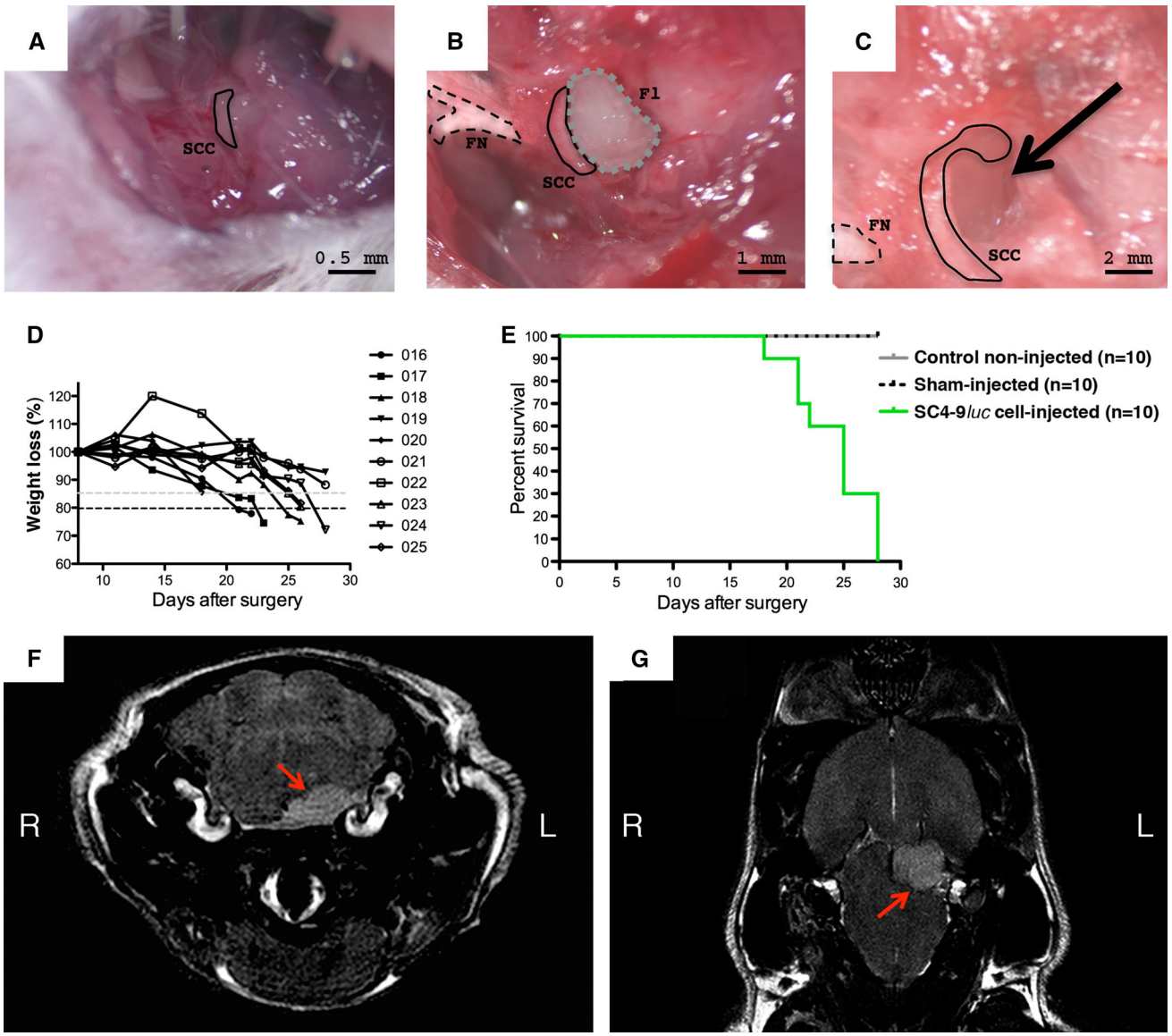

Fig. 1 Microsurgical approach to the auditory-vestibular nerve complex in mice. **a–c** Intraoperative view showing the lateral skull base. **a** A retro-auricular approach allowed exposure of the lateral semi-circular canal (SSC, *black line*). **b** The bone overlying the flocculus (Fl, *dashed gray line*) in the proximity of the extracranial facial nerve (FN, *dashed black line*) was drilled and the flocculus retracted postero-superiorly allowing access to the cysterna pontis. **c** The ampulla of the lateral semi-circular canal maps the entry of the superior vestibular nerve in the otic capsule and was used as a reliable landmark to proceed with targeted cell injection (*arrow*). **d** After recovering from surgery, SC4-9*luc* cell-injected mice progressively lost weight, but accelerating weight loss after day 20 following surgery lead to euthanasia (*dashed gray line*: 15 % of body weight loss, *dashed back line*: 20 % of body weight loss). **e** Cell-injected mice showed a median survival of 25 days following surgery, whereas no death was accounted for in the sham-injected or control groups. **f–g** Three weeks after surgical grafting, MRI coronal (F) and axial (G) sequences demonstrated engraftment of the SC4-9*luc* cells in the cerebellopontine angle with involvement of the inner auditory canal and mass effect on the brainstem, mimicking the human condition

Precision Instruments) and a 34 Gauge titanium 25 degree beveled tip needle.

Bioluminescence imaging

The growth of SC4-9*luc* orthotopic allografts was monitored by bioluminescence imaging using the IVIS imaging system (Caliper, PerkinElmer). All images were obtained 12 min after intraperitoneal injection of firefly luciferin (I.P., 225 mg/kg, Caliper) within a 60-180 s time acquisition. Mice were sedated continuously via inhalation of 2.5 % isoflurane (Abbott Laboratories Ltd.). 2D BLI image datasets were analyzed using Living Image 4.2 software (Caliper, PerkinElmer). Standard round-shaped region of

interest (ROI) was centered on the maximum emitted radiance and average radiance (photons/s/cm2/sr) calculated for each animal.

Magnetic resonance imaging

Anesthesia was induced and maintained with isoflurane throughout the imaging procedure. Mice were inserted in the prone position into a small animal MRI scanner (PharmaScan 300, Bruker BioSpin Division) 7T magnet using the 19-mm inner diameter transmit receive coil. ParaVision 4.0 scanner software (BRUKER BioSpin MRI GmbH) was set to use RARE (Rapid Acquisition with Relaxation Enhancement) spin echo sequence for fast T2-weighted imaging (echo time = 50, repetition time = 3000, RARE Factor 8) with a 256 × 256 in-plane matrix and 2.56 cm field of view. After scanning, if needed, mice were gently warmed on a thermostatically controlled heating pad until awake enough to be returned to their home cage. MRI images were reconstructed at native resolution. For each mouse, we acquired 22 axial images with 0.4 mm thick slices and 0.02 mm gap between slices. This produced 0.1 × 0.1 mm^2 per pixel in-plane resolution with an effective slice thickness of 0.42 mm. eFilm Workstation 1.8.1 (eFilm Medical Inc.) was used to transfer reconstructed images into DICOM files. The volume of the tumors were measured by manual segmentation using the OsiriX image analysis software [23].

Auditory brainstem responses (ABR) for objective assessment of auditory thresholds in mice

Mice were anesthetized by intraperitoneal administration of xylazine (10 mg/kg) and ketamine-HCl (100 mg/kg). During ABR measurement, body temperature was kept at 38 °C with a heating pad. Stainless steel needle electrodes were placed on the vertex and below the ipsilateral ear, with ground electrode on the body of the anesthetized mice. Impedance was checked (below 5 kΩ) after positioning the set of electrodes. Tone-pips were elicited ranging from 4 to 32 kHz to obtain frequency specific information. Multiple repetitions of stimuli (300) were yield to obtain an averaged waveform. The recorded signals were bandpass filtered (300 to 3000 Hz) and amplified with a differential amplifier (105 μV). ABRs were recorded and reviewed with BioSig software (Tucker Davis Technologies). The threshold was defined as the lowest level at which waves of the ABR could be clearly detected by visual inspection. All thirty age matched mice in the surgery experimental group were tested following the same protocol on both ears. Testing was set at 7 weeks of age for baseline (before surgery) and 2, 14, and 21 days after surgery. Twenty ears of 10 non-injected control mice were tested all along as controls. In the cell-injected group (10 mice) the non-operated ears were tested as 10 more control ears. In the sham-injected group (10 mice) the non-operated ears were tested as 10 more control ears.

Histopathology

Whole mouse heads were dissected and skull fixed in 4 % paraformaldehyde (PFA) for 24 h, then decalcified for 24 h (RapidCal-Immuno™, BBC biochemical corporation) and embedded in paraffin. Each specimen was sectioned at 3.5 μm thickness and stained with standard H&E as previously described [24].

Data analysis

For measurements, data are expressed as mean ± SEM. For statistical comparison at the end-point we used a Student *t* test with the level of significance set at $p < 0.05$ (two-tailed). Statistical calculations were done using GraphPad, Prism 5.0a. The correlation between tumor size and the average radiance in photon/sr/cm^2 was evaluated using a linear regression.

Results

Microsurgical approach to the auditory-vestibular nerve complex

For the cell-derived allograft in this study we chose the SC4 cell line that has become a standard in NF2 basic and preclinical research [21, 25, 26]. SC4 cells were labeled with luciferase so that in vivo bioluminescence imaging could be applied to longitudinally monitor orthotopic tumor growth across the study. A microsurgical approach was utilized to graft SC4-9*luc* cells in the region of the auditory-vestibular (8th) nerve complex in the cerebellopontine angle. Thirty NU/NU mice were divided in three groups: the allograft group was injected with the SC4-9*luc* cell suspension, the sham surgery group that received the same volume of the cell-free medium as the allograft group, and the control group with no surgery. No death was recorded during or directly after surgery. In the SC4-9*luc* cell-injected group all mice developed a tumor. After recovering from surgery, mice progressively lost weight and reached a clinical endpoint requiring euthanasia 20 days after surgery (Fig. 1d). The median survival was 25 days in the allograft group. Survival was not affected by sham injection compared to the control group with no surgery (Fig. 1e). To monitor the kinetic of tumor growth, bioluminescence imaging (BLI) and MRI (Fig. 1f–g) were sequentially acquired. We found that tumor bearing mice could be readily identified using both methods (Fig. 3a, b), however

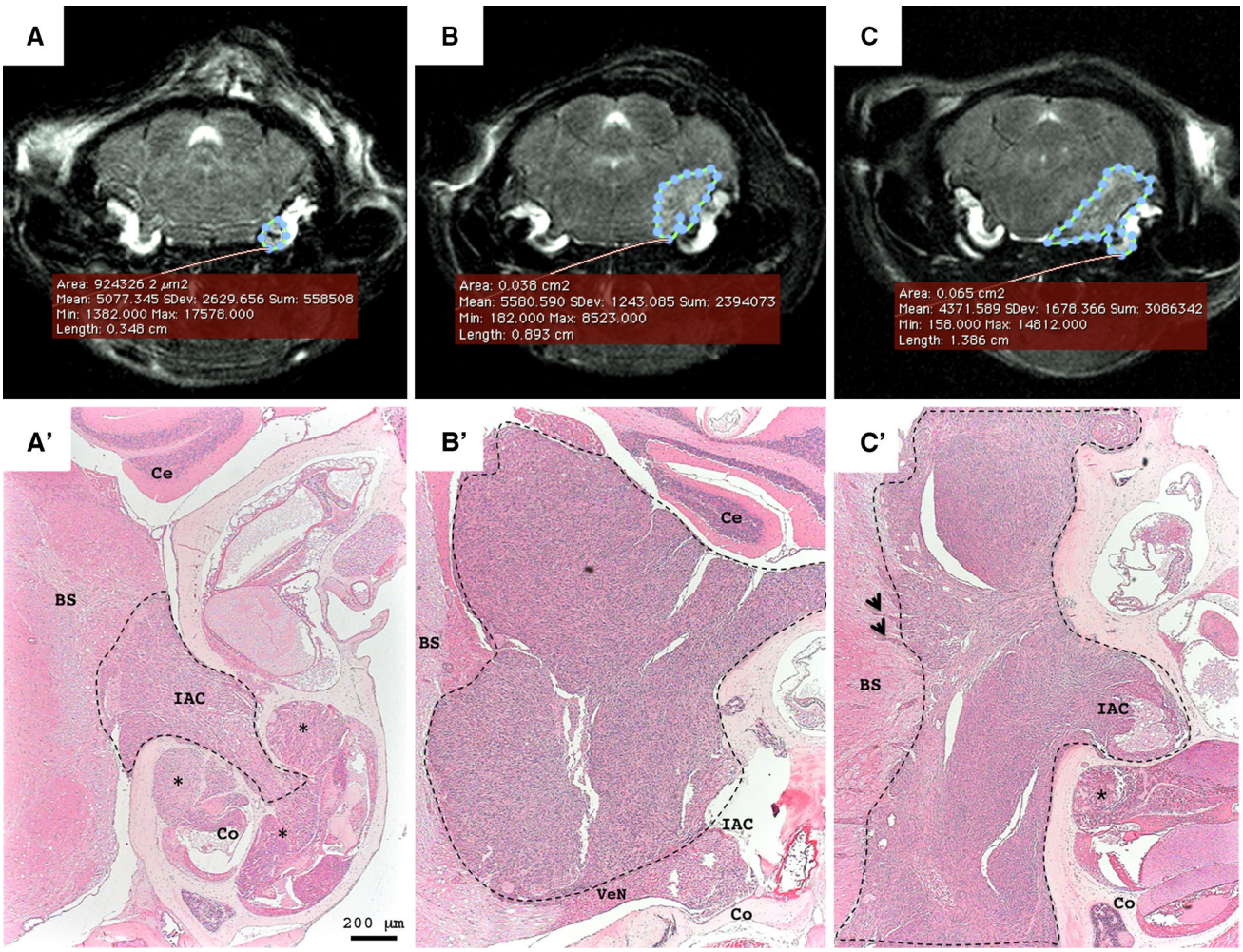

Fig. 2 Location of tumors following SC4-9*luc* cell injection by stereotactic approach. **a–c** MRI scans showing SC4-9*luc* tumors (*blue line*) located in the inner auditory canal and midturn of the left cochlea (Co) (**a**), in the cerebellopontin angle (**b**) and compressing the brainstem (**c**). **a′–c′** Histological sections of the MRI-scanned mice at the level of the inner auditory canal (IAC). **a′** The resulting tumor proliferated in the 8th cranial nerve at the level of the IAC with intracochlear extension (*asterisks*) through the modiolus. **b′** Tumor extended in the cerebellopontine angle brainstem (BS), respecting the arachnoidal layer that covers the flocculus of the cerebellum (Ce). Note the vestibular nerve (VeN) in the lower part of the image. **c′** Tumor at a later stage demonstrating an aggressive cell phenotype with brainstem invasion (*arrowheads*)

we noticed a discrepancy between BLI signal and MR measurements of tumor size. Although BLI can detect tumor growth early after implantation (tumor volume <5 mm^3), in mice with larger tumors (>5 mm^3), increasing MR volumes did not correlate with average emitted radiance that tended to plateau. A similar effect, with in vivo BLI signal plateauing in large tumors, has been observed previously and is generally attributed to development of hemorrhage and necrosis within the tumor bed [27, 28].

Stereotactic approach to the auditory-vestibular nerve complex

As an alternative to microsurgery, we developed a stereotactic approach to reduce operator-induced variables and accurately reproduce the site of grafting. Twenty NU/NU mice were divided in two groups and operated using this approach. One group received the SC4-9*luc* cell suspension, the other group was sham injected with the same volume of cell-free medium. No death was recorded secondary to the injection. Tumor growth was monitored twice a week using thin cut MRI to determine tumor onset and growth characteristics. In the group of mice injected with the SC4-9*luc* cell suspension, 8 of 10 mice monitored by MRI developed a tumor of the 8th cranial nerve extending in the inner auditory canal and cerebellopontine angle, thereby closely mimicking the human condition (Fig. 2). Tumors could be detected as early as day 11 (0.32 ± 0.08 mm^3) and tumor growth was followed up to 21 days (2.7 ± 0.9 mm^3) after stereotactic grafting when

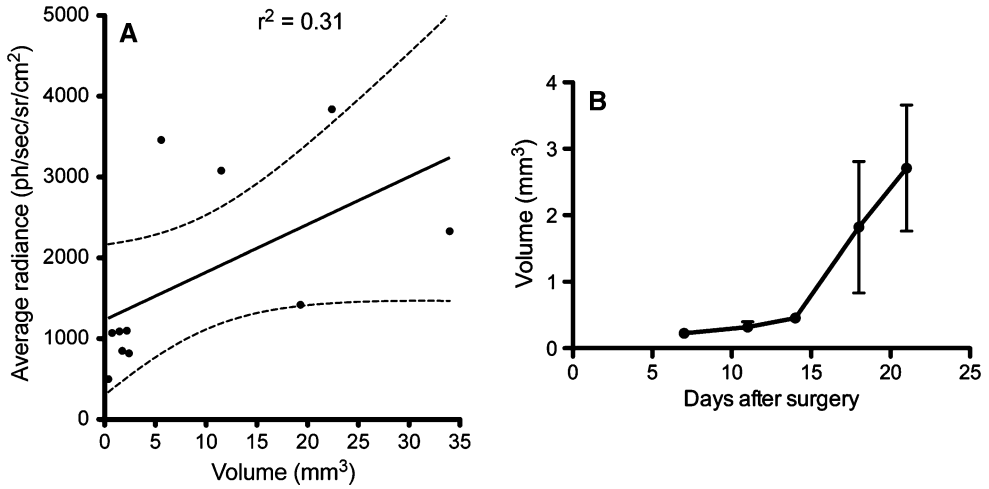

Fig. 3 Follow-up of SC4-9*luc* tumor growth by bioluminescence imaging (BLI) and MRI. **a**, **b** For each mouse tumor generated by microsurgical injection of luciferase-bearing SC4-9*luc* cells, BLI average radiance was plotted versus corresponding MRI-determined volume. **a** A trend toward a linear correlation existed between BLI and MRI measurements, though it did not reach the statistical significance ($r^2 = 0.31$), with in vivo BLI signal plateauing in large tumors. **b** Longitudinal monitoring of tumor growth by MRI in 8 NU/NU mice after SC4-9*luc* cell injection by stereotactic approach. Volume measurements were obtained using a manual trace method where tumor borders were manually outlined in each image slice. The volume calculation algorithm in OsiriX was used to obtain a three-dimensional tumor volumetric measurement (mm^3)

mice developed clinical signs indicative of a moribund condition requiring euthanasia. The average tumor growth rate from day 11 to day 21 was 0.28 mm^3/day (Fig. 3c). In all analyzed cases, the main causes of death were the extension of the tumor into the otic capsule and compression of neighboring structures by tumor expansion. Control mice in the sham injected group did not show reduced survival.

Monitoring the effect of SC4-9luc tumor growth on auditory function in NU/NU mice

Consistent hearing levels were observed across 7-week-old NU/NU mice tested before any surgical procedure ($n = 30$, 60 ears total), with no significant intra-individual differences (Fig. 4a). Two days after surgery a general worsening of hearing in both sham- and cell-injected mice was recorded, with an increase in thresholds prevailing on the low frequencies (4 and 8 kHz) (Fig. 4b) suggesting a pressure mechanism secondary to CSF depletion. Hearing recovery in the sham-injected group occurred progressively up to day 14 after surgery when thresholds matched those of the non-injected control group (Fig. 4c). However, in the cell-injected mice a increased threshold at 16 kHz was observed and low-frequency hearing loss did not revert to the levels observed in non-injected, and sham-injected mice. This difference was statistically significant and increased at day 21 (*t* test, $p < 0.05$, $n = 10$ each group) (Fig. 4d). Interestingly, between 8 and 11 weeks of age, the non-injected control NU/NU mice showed early progressive high-frequency hearing loss (24 kHz, Fig. 4b–d), suggestive of early presbicusis in this mouse strain. In conclusion, in the NU/NU;SC4-9*luc* allograft model, the 16 kHz frequency appeared to be the most reliable measurement since it demonstrated specific and significant progressive hearing loss from day 2 to day 21 after surgery in the allografted mice and was neither affected by aging (at least up to 11 weeks of age), nor by surgery.

Discussion

Since Lee et al. introduced in 1992 the possibility of grafting fresh human vestibular schwannoma specimens in nude mice while maintaining survival and growth in a specific tissue environment, little progress has been made to enable the use of such models to further study schwannoma biology [29]. In fact, only few other publications used xenografts of fresh human specimens as models for schwannoma growth [30–32]. Interestingly, Neff et al. proposed a stereotactic approach to graft freshly isolated schwannoma cells into the caudate nucleus of NOD/SCID mice followed by in vivo BLI [33]. Although not reproducing the original location of vestibular schwannoma, this approach eventually provided information on the impact of blood brain barrier. Nevertheless, a low grafting rate and absence of discrete tumor growth limit its use.

Our study was designed to provide a proof of principle for grafting schwannoma cells in the acoustico-facial nerve

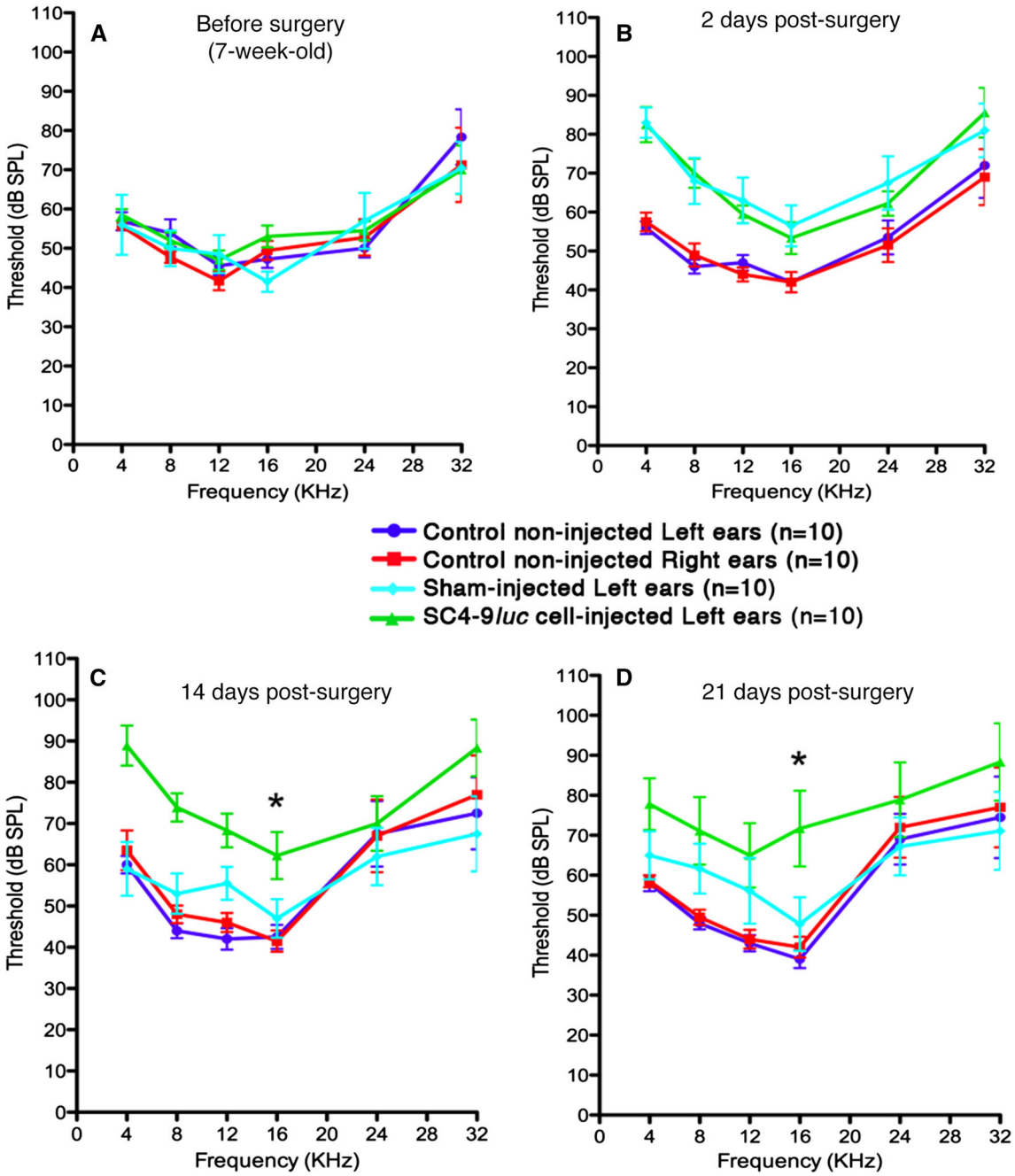

Fig. 4 Auditory brainstem responses (ABRs) measurements for objective testing of auditory function. Average ABRs evoked by an acoustic stimuli (Tone-pips, 4–32 kHz) delivered at decreasing intensities (dB SPL), bandpass filtered (300–3000 Hz) and amplified with a differential amplifier (105 μV). ABRs obtained in 10 control non-injected NU/NU mice (*left* and *right ears*), 10 sham-injected NU/NU mice (*left ears*) and 10 SC4-9*luc* cell-injected NU/NU mice (*left ears*) before surgery (**a**, 7 week-old), 2 days after surgery (**b**, 8 week-old), 14 days after surgery (**c**, 10 week-old), 21 days after surgery (**d**, 11 week-old). A statistically significant shift at 16 kHz is observed in SC4-9*luc* tumor-bearing mice (*left ears*) compared to sham-injected mice (*left ears*) starting 14 days after surgery (*t* test, $p < 0.05$)

complex region, using the SC4-9 cell line. SC4-9 has become a standard model in NF2 research since it recapitulates signalling network signatures of human and mouse NF2 schwannomas [19, 21, 25, 26], with high grafting efficiency when orthotopically injected into the sciatic nerves of immunodeficient NU/NU mice [34]. We found that the microsurgical approach successfully targeted the anatomic location where human VS predominantly arise and tumor development could be monitored by in vivo imaging. We also showed that by using carefully identified stereotactic coordinates, precise targeting of the auditory-vestibular complex region can be achieved, thus

limiting operator-induced variables. This is particularly relevant in the context of using mouse and human VS allograft models for high throughput drug evaluation and to inform trial design in more sophisticated GEM NF2 models. In vivo imaging and histological analysis showed that SC4-9 tumors developed in the cerebello-pontine region with similar extensions as human VS. These included intracochlear localization and brainstem compression eventually causing death. The use of other mouse and human cellular models, including slow-growing primary VS cells, will eventually mimick the benign, indolent nature of human VS. For each new VS cell model grafted in vivo using this approach, the natural history of allograft tumor development can be analyzed by MRI. This will define the cell line-specific time frame in which tumor growth is limited to the anatomical region of interest, making new models suitable for preclinical drug testing using tumor volume and hearing as endpoints.

One of the limitations of this model is that the transient hearing loss observed in both the surgical and non-surgical (contralateral) ears was likely due to the surgical technique, which requires opening of the arachnoidal layer at the level of the cerebellopontine angle to deplete cerebrospinal fluid (CSF) from cysterna pontis and/or magna. The effect of changes in the CSF pressure on hearing has been widely documented in clinical reports [35–37]. More precisely, in humans, hearing loss affects preferentially low frequencies (125–500 Hz) and high frequencies (4000–8000 Hz), whereas medium frequencies (2000 Hz) are well respected. The lower frequencies tend to take more time to recover. Subsequently, this early shift was reproduced in animal models with depletion of perilymphatic fluids or CSF [38]. The rapid tumor growth with intra-cochlear extension is likely the primary cause of hearing loss in the SC4-9 model. Intracochlear extension has been described for human VS, although its prevalence among NF2 patient is yet to be determined [39, 40]. Use of VS cell lines with different growth patterns might become relevant to dissect other causes of hearing loss in these patients, in addition to tumor compression of the acoustic nerve.

The most frequent hearing finding in pure tone audiometry for VS in humans is a high frequency sensorineural hearing loss [7, 8, 41]. Animal models cannot precisely recapitulate hearing loss in humans since other mammalians do not share our unique auditory sensitivity [42]. In this study we used tone pips for frequency-specific testing within the mouse auditory spectrum. We observed a specific threshold increase at 16 kHz consistent with the increased thresholds in the higher frequencies observed in the human condition. Because of the early occurrence of presbycusis in this mouse strain, the effect of tumor growth on higher frequencies could not be determined. Use of genetic backgrounds of immunodeficient mice with different hearing characteristics could help address this issue.

The report of a favorable impact of an anti-angiogenic treatment on hearing in NF2 VS patients compels the need to understand the relationship between VS growth and hearing loss [16]. As a result, hearing outcome during treatment has became the primary endpoint for clinical trials investigating antiangiogenic compounds such as bevacizumab. Thus, the inclusion of a hearing endpoint in VS preclinical trials using a varity of cellular models will contribute to the characterization of compound efficacy and prioritization.

Acknowledgments We thank Rosa Sierra and Erica Canal for technical support.

Funding This study was funded by a Young Investigator Award (N-X.B.) and by the Neurofibromatosis Preclinical Consortium of the Children's Tumor Foundation; Advocure NF2 Inc. and by the House Research Institute.

Compliance with ethical standards

Conflict of Interest The authors declare that they have no conflict of interest.

References

1. Kshettry VR, Hsieh JK, Ostrom QT, Kruchko C, Barnholtz-Sloan JS (2015) Incidence of vestibular schwannomas in the United States. J Neurooncol 124:223–228. doi:10.1007/s11060-015-1827-9
2. Evans DG, Moran A, King A, Saeed S, Gurusinghe N, Ramsden R (2005) Incidence of vestibular schwannoma and neurofibromatosis 2 in the North West of England over a 10-year period: higher incidence than previously thought. Otol Neurotol 26:93–97
3. Rouleau GA, Merel P, Lutchman M, Sanson M, Zucman J, Marineau C, Hoang-Xuan K, Demczuk S, Desmaze C, Plougastel B et al (1993) Alteration in a new gene encoding a putative membrane-organizing protein causes neuro-fibromatosis type 2. Nature 363:515–521. doi:10.1038/363515a0
4. Trofatter JA, MacCollin MM, Rutter JL, Murrell JR, Duyao MP, Parry DM, Eldridge R, Kley N, Menon AG, Pulaski K et al (1993) A novel moesin-, ezrin-, radixin-like gene is a candidate for the neurofibromatosis 2 tumor suppressor. Cell 72:791–800
5. Bijlsma EK, Merel P, Bosch DA, Westerveld A, Delattre O, Thomas G, Hulsebos TJ (1994) Analysis of mutations in the SCH gene in schwannomas. Genes Chromosom Cancer 11:7–14
6. Hadfield KD, Smith MJ, Urquhart JE, Wallace AJ, Bowers NL, King AT, Rutherford SA, Trump D, Newman WG, Evans DG (2010) Rates of loss of heterozygosity and mitotic recombination in NF2 schwannomas, sporadic vestibular schwannomas and schwannomatosis schwannomas. Oncogene 29:6216–6221. doi:10.1038/onc.2010.363
7. Harner SG, Fabry DA, Beatty CW (2000) Audiometric findings in patients with acoustic neuroma. Am J Otol 21:405–411
8. Tutar H, Duzlu M, Goksu N, Ustun S, Bayazit Y (2012) Audiological correlates of tumor parameters in acoustic neuromas. Eur Arch Otorhinolaryngol. doi:10.1007/s00405-012-1954-2

9. van de Langenberg R, de Bondt BJ, Nelemans PJ, Dohmen AJ, Baumert BG, Stokroos RJ (2011) Predictors of volumetric growth and auditory deterioration in vestibular schwannomas followed in a wait and scan policy. Otol Neurotol 32:338–344. doi:10.1097/MAO.0b013e3182040d9f
10. Asthagiri AR, Vasquez RA, Butman JA, Wu T, Morgan K, Brewer CC, King K, Zalewski C, Kim HJ, Lonser RR (2012) Mechanisms of hearing loss in neurofibromatosis type 2. PLoS One 7:e46132. doi:10.1371/journal.pone.0046132
11. Fisher LM, Doherty JK, Lev MH, Slattery WH (2009) Concordance of bilateral vestibular schwannoma growth and hearing changes in neurofibromatosis 2: neurofibromatosis 2 natural history consortium. Otol Neurotol 30:835–841. doi:10.1097/MAO.0b013e3181b2364c
12. Mahmud MR, Khan AM, Nadol JB Jr (2003) Histopathology of the inner ear in unoperated acoustic neuroma. Ann Otol Rhinol Laryngol 112:979–986
13. Warren FM 3rd, Kaylie DM, Aulino JM, Jackson CG, Weissman JL (2006) Magnetic resonance appearance of the inner ear after hearing-preservation surgery. Otol Neurotol 27:393–397
14. Stankovic KM, Mrugala MM, Martuza RL, Silver M, Betensky RA, Nadol JB Jr, Stemmer-Rachamimov AO (2009) Genetic determinants of hearing loss associated with vestibular schwannomas. Otol Neurotol 30:661–667. doi:10.1097/MAO.0b013e3181a66ece
15. Evans DG (2009) Neurofibromatosis type 2 (NF2): a clinical and molecular review. Orphanet J Rare Dis 4:16. doi:10.1186/1750-1172-4-16
16. Plotkin SR, Stemmer-Rachamimov AO, Barker FG 2nd, Halpin C, Padera TP, Tyrrell A, Sorensen AG, Jain RK, di Tomaso E (2009) Hearing improvement after bevacizumab in patients with neurofibromatosis type 2. N Engl J Med 361:358–367. doi:10.1056/NEJMoa0902579
17. Patel MM, Goyal BR, Bhadada SV, Bhatt JS, Amin AF (2009) Getting into the brain: approaches to enhance brain drug delivery. CNS Drugs 23:35–58. doi:10.2165/0023210-200923010-00003
18. Giovannini M, Robanus-Maandag E, van der Valk M, Niwa-Kawakita M, Abramowski V, Goutebroze L, Woodruff JM, Berns A, Thomas G (2000) Conditional biallelic Nf2 mutation in the mouse promotes manifestations of human neurofibromatosis type 2. Genes Dev 14:1617–1630
19. Lallemand D, Manent J, Couvelard A, Watilliaux A, Siena M, Chareyre F, Lampin A, Niwa-Kawakita M, Kalamarides M, Giovannini M (2009) Merlin regulates transmembrane receptor accumulation and signaling at the plasma membrane in primary mouse Schwann cells and in human schwannomas. Oncogene 28:854–865. doi:10.1038/onc.2008.427
20. Manent J, Oguievetskaia K, Bayer J, Ratner N, Giovannini M (2003) Magnetic cell sorting for enriching Schwann cells from adult mouse peripheral nerves. J Neurosci Methods 123:167–173
21. Morrison H, Sperka T, Manent J, Giovannini M, Ponta H, Herrlich P (2007) Merlin/neurofibromatosis type 2 suppresses growth by inhibiting the activation of Ras and Rac. Cancer Res 67:520–527. doi:10.1158/0008-5472.CAN-06-1608
22. Wu M, Wallace MR, Muir D (2005) Tumorigenic properties of neurofibromin-deficient Schwann cells in culture and as syngrafts in Nf1 knockout mice. J Neurosci Res 82:357–367. doi:10.1002/jnr.20646
23. Rosset A, Spadola L, Ratib O (2004) OsiriX: an open-source software for navigating in multidimensional DICOM images. J Digit Imaging 17:205–216. doi:10.1007/s10278-004-1014-6
24. Stemmer-Rachamimov AO, Louis DN, Nielsen GP, Antonescu CR, Borowsky AD, Bronson RT, Burns DK, Cervera P, McLaughlin ME, Reifenberger G, Schmale MC, MacCollin M, Chao RC, Cichowski K, Kalamarides M, Messerli SM, McClatchey AI, Niwa-Kawakita M, Ratner N, Reilly KM, Zhu Y, Giovannini M (2004) Comparative pathology of nerve sheath tumors in mouse models and humans. Cancer Res 64:3718–3724. doi:10.1158/0008-5472.CAN-03-4079
25. Hennigan RF, Moon CA, Parysek LM, Monk KR, Morfini G, Berth S, Brady S, Ratner N (2013) The NF2 tumor suppressor regulates microtubule-based vesicle trafficking via a novel Rac, MLK and p38(SAPK) pathway. Oncogene 32:1135–1143. doi:10.1038/onc.2012.135
26. Kim JY, Song JJ, Kwon BM, Lee JD (2015) Tanshinone IIA exerts antitumor activity against vestibular schwannoma cells by inhibiting the expression of hypoxia-inducible factor-1alpha. Mol Med Rep 12:4604–4609. doi:10.3892/mmr.2015.3932
27. Jost SC, Collins L, Travers S, Piwnica-Worms D, Garbow JR (2009) Measuring brain tumor growth: combined bioluminescence imaging-magnetic resonance imaging strategy. Mol Imaging 8:245–253
28. Sarraf-Yazdi S, Mi J, Dewhirst MW, Clary BM (2004) Use of in vivo bioluminescence imaging to predict hepatic tumor burden in mice. J Surg Res 120:249–255. doi:10.1016/j.jss.2004.03.013
29. Lee JK, Sobel RA, Chiocca EA, Kim TS, Martuza RL (1992) Growth of human acoustic neuromas, neurofibromas and schwannomas in the subrenal capsule and sciatic nerve of the nude mouse. J Neurooncol 14:101–112
30. Linskey ME, Martinez AJ, Kondziolka D, Flickinger JC, Maitz AH, Whiteside T, Lunsford LD (1993) The radiobiology of human acoustic schwannoma xenografts after stereotactic radiosurgery evaluated in the subrenal capsule of athymic mice. J Neurosurg 78:645–653. doi:10.3171/jns.1993.78.4.0645
31. Chang LS, Jacob A, Lorenz M, Rock J, Akhmametyeva EM, Mihai G, Schmalbrock P, Chaudhury AR, Lopez R, Yamate J, John MR, Wickert H, Neff BA, Dodson E, Welling DB (2006) Growth of benign and malignant schwannoma xenografts in severe combined immunodeficiency mice. Laryngoscope 116:2018–2026. doi:10.1097/01.mlg.0000240185.14224.7d
32. Clark JJ, Provenzano M, Diggelmann HR, Xu N, Hansen SS, Hansen MR (2008) The ErbB inhibitors trastuzumab and erlotinib inhibit growth of vestibular schwannoma xenografts in nude mice: a preliminary study. Otol Neurotol 29:846–853. doi:10.1097/MAO.0b013e31817f7398
33. Neff BA, Voss SG, Allen C, Schroeder MA, Driscoll CL, Link MJ, Galanis E, Sarkaria JN (2009) Bioluminescent imaging of intracranial vestibular schwannoma xenografts in NOD/SCID mice. Otol Neurotol 30:105–111. doi:10.1097/MAO.0b013e31818b6cea
34. Giovannini M, Bonne NX, Vitte J, Chareyre F, Tanaka K, Adams R, Fisher LM, Valeyrie-Allanore L, Wolkenstein P, Goutagny S, Kalamarides M (2014) mTORC1 inhibition delays growth of neurofibromatosis type 2 schwannoma. Neuro Oncol 16:493–504. doi:10.1093/neuonc/not242
35. Walsted A, Nielsen OA, Borum P (1994) Hearing loss after neurosurgery. The influence of low cerebrospinal fluid pressure. J Laryngol Otol 108:637–641
36. Walsted A, Salomon G, Olsen KS (1991) Low-frequency hearing loss after spinal anesthesia. Perilymphatic hypotonia? Scand Audiol 20:211–215
37. Walsted A, Salomon G, Olsen KS (1993) Hearing loss after spinal anesthesia. An audiological controlled trial. Ugeskr Laeger 155:3009–3011
38. Walsted A, Nilsson P, Gerlif J (1996) Cerebrospinal fluid loss and threshold changes. 2. Electrocochleographic changes of the compound action potential after CSF aspiration: an experimental study. Audiol Neurootol 1:256–264

39. Nam SI, Linthicum FH Jr, Merchant SN (2011) Temporal bone histopathology in neurofibromatosis type 2. Laryngoscope 121:1548–1554. doi:10.1002/lary.21822
40. Doherty J, Go JL, Linthicum FH Jr (2014) Neurofibromatosis 2 invasion of the internal auditory canal wall: clinical significance. Otol Neurotol 35:1662–1668. doi:10.1097/MAO.0000000000000494
41. Morlet T, Dubreuil C, Duclaux R, Ferber-Viart C (2003) Pre-operative speech and pure-tone audiometry in four types of patients with acoustic neuroma. Am J Otolaryngol 24:297–305
42. Vater M, Kossl M (2011) Comparative aspects of cochlear functional organization in mammals. Hear Res 273:89–99. doi:10.1016/j.heares.2010.05.018